Synergistic photoredox and copper catalysis by diode-like coordination polymer with twisted and polar copper-dye conjugation

Yusheng Shi
Dalian University of Technology
Tiexin Zhang
Dalian University of Technology
Xiao-Ming Jiang
Fujian Institute of Research on the Structure of Matter
Gang Xu
Fujian Institute of Research on the Structure of Matter, Chinese Academy of Sciences
Cheng He
Dalian University of Technology
Chunying Duan (cyduan@dlut.edu.cn)
Dalian University of Technology https://orcid.org/0000-0003-1638-6633

Article

Keywords: synergistic photoredox, copper catalysis, Cu(II), photoelectronic behavior

Posted Date: July 24th, 2020

DOI: https://doi.org/10.21203/rs.3.rs-43961/v1

Version of Record: A version of this preprint was published at Nature Communications on October 23rd, 2020. See the published version at https://doi.org/10.1038/s41467-020-19172-3.

Abstract

Synergistic photoredox and copper catalysis confers new synthetic possibilities in pharmaceutical field, but is seriously affected by the consumptive fluorescence quenching of Cu(II). By decorating bulky auxiliaries into photoreductive triphenylamine-based ligand to twist the conjugation between triphenylamine-based ligand and polar Cu(II)-carboxylate node in coordination polymer, we reported a heterogeneous approach to directly confronting this inherent problem. The twisted and polar Cu(II)-dye conjunction endowed coordination polymer with diode-like photoelectronic behaviours, which hampered the inter- and intramolecular photoinduced electron transfer from triphenylamine-moiety to Cu(II) site and permitted the reversed-directional ground-state electronic conductivity, rectifying the productive loop circuit for synergising photoredox and copper catalysis in pharmaceutically valuable decarboxylative C(sp^3)-heteroatom couplings. The well-retained Cu(II) sites during photoirradiation exhibited unique inner-spheric modulation effects, which endowed the couplings with adaptability to different types of nucleophiles and radical precursors under concise reaction conditions, and distinguished the multi-olefinic moieties of biointeresting steride derivatives in their late-stage trifluoromethylation-chloration difunctionalisation.

Introduction

C(sp^3)-heteroatom bond formation is of fundamental importance in pharmaceutical fields, however remains one of the major challenges in the fields of cross-coupling chemistry.[1] Taking advantage of the multiple valance states, Cu(II) catalysts enable the capture of single-electronic carbon-centred radicals, and the following facile reductive elimination to realize the key steps of cross couplings.[2] The synergy of photoredox and copper catalysis provides a sustainable way to generate radicals for conducting C(sp^3)-heteroatom couplings.[3,4] The major challenging limits the direct combination of photoredox and copper catalysis was the strong quenching effect of Cu(II) ions towards the highly reductive excited states of photosensitizers that required for the radical generation.[5] In practice, photoredox and copper catalysis are usually compromised by adopting the high loadings of Cu(I) precursors to kinetically balanced off the excited-state quenching effect of *in situ* generated Cu(II) ions.[6–8] Thinking outside the box by a manner of aggregation state, the crystalline porous coordination polymers[9,10] fix photosensitizers and copper(II) ions in high local concentrations and spatially isolate them to block the futile intermolecular fluorescence quenching (Fig. 1b). Moreover, the electronic communications between chromophore-based ligands and Cu(II) nodes could be regulated to hamper the intramolecular fluorescence quenching. The well-modified Cu(II)-dye coordination polymers would directly confront the inherent requirements of this regime in a heterogeneous manner and simultaneously circumvent the risk of residual heavy metals that caused by high loadings of Cu(I) salts.

The pioneering results revealed that the connection modes between photosensitizers and redox-active metals in coordination supramolecular systems[11,12] vitally affect the electron transfer routes between both entities. The direct connection by a conjugative linkage permits the molecular wire-like bidirectional

electronic conductivity at both excited and ground states,[13] which impairs its catalytic applications. Twisting the conjugative junction between the electron-donating and accepting sections within a single-molecule device was shown to markedly enhance the charge transfer resistance.[14,15] Noted that higher reorganization energy was required for one-way electron transfer through the high-polar carboxylate–metal node in the most common carboxylate-based coordination polymers.[16] Moreover, as a versatile photosensitiser, triphenylamine (**TPA**) has been successfully modified into carboxylate-based coordination polymers to generate radicals by photoreduction.[17] Thus, the twisted conjugative connection of **TPA**-based ligand and polar carboxylate–copper node might realize the diode-like unidirectional electronic conductivity within coordination polymer for compromising photoredox and copper catalysis.[18] Herein, we showed a new approach to modifying the electronic communications in the Cu(II)–**TPA** coordination polymer by introducing a bulky group at the *ortho*-position of the phenylcarboxylic coordination group of **TPA**-based ligand to twist the π-conjugation between phenyl moiety and the coordinated carboxylate (Fig. 1a). We envisioned that this special series connection of twisted conjugation and polar carboxylate–copper node within Cu(II)–**TPA** coordination polymer should kinetically alleviate the inter- and intramolecular photoinduced electron transfer (PET) from the excited-state **TPA** fragment to Cu(II) ion.[19] The ground-state electronic communication thermodynamically allows the alternative directional single electron transfer (SET) from the *in situ* formed Cu(I) to the oxidized **TPA** moiety (Fig. 1c).[20] This molecular diode-like behaviour of twisted conjugation and polar node rectifies the productive loop-circuit electron transfer route that required by synergizing the photoredox and copper catalytic cycles (Fig. 1c).

Considering the value of decarboxylative C(sp^3)-heteroatom couplings in the pharmaceutical field[21] and their reliance on both photocatalyitc radical generation and Cu(II)-catalytic radical capture as well as the following reductive elimination, the decarboxylative C(sp^3)-N couplings between iodonium carboxylate-type alkyl radical precursors and *N*-centred heterocycles were examined as a proof-of-concept of the diode-like Cu(II)–**TPA** coordination polymer for synergising photoredox and copper catalysis (Fig. 1d). Taking advantages of Cu(II) centres that retained during the PET processes to exert the possible activation to the ester moiety, this synergistic catalysis was further extended to the use of more challenging *N*-hydroxyphthalimide esters as alkyl radical precursors for the value-added C(sp^3)-N/O/S couplings with aniline/phenol/thiophenol nucleophiles, respectively. Moreover, this unique activation of the enriched ground-state Cu(II) sites was further unveiled to successfully distinguish the multiple olefinic moieties in the late-stage trifluoromethylation-chloration difunctionalisation of olefins within biointeresting steride derivatives.[22,23]

Results

Synthesis and characterisation of Cu(II)-dye coordination polymers. The installation of a chiral oxazolidinone moiety[24] at *ortho*-position of carboxylic linker of the typical **TPA**-based ligand tris(4'-carboxybiphenyl)amine (named as H_3**L-Planar**) afforded a new ligand tris[4-(4-carboxy-3-((*R*)-4-isopropyl-

2-oxooxazolidin-3-yl)-phenyl)phenyl]amine (named as H_3**L-Twisted**). The coordination polymer Cu–**Twisted** was obtained in a 70% yield by the solvothermal reaction between $Cu(NO_3)_2$• $3H_2O$ and H_3**L-Twisted** at 80 ^oC for 3 days. Cu–**Twisted** consisted of truncated cubic cages (internal diameter *ca*. 2.9 nm, Fig. S2), each delimited by eight **L-Twist**$^{3-}$ linkers and twelve $Cu_2(O_2C)_4$ paddle-wheels, forming dumbbell-shaped 1D channels with a cross-sectional area of 15 × 27 $Å^2$ along the *a*-direction (Fig. 2b).[25] The free volume of desolvated Cu–**Twisted** was estimated as *ca*. 62% of the porous polymer, and a Brilliant Blue R-250 dye uptake experiment with Cu–**Twisted** yielded a 54% absorption amount of the coordination polymer weight as determined by UV-Vis spectroscopy (Fig. S9), implying the possibility of accommodating substrates and reagents within the pores.[26] The steric hindrance between the bulky oxazolidinone and the $Cu_2(O_2C)_4$ paddle-wheel forged a twisted dihedral angle between the conjugated carboxylic coordination group and the adjacent phenyl moiety (Fig. 2a),[27] which induced the symmetry of coordination polymer into a **pto** lattice (Figs. 2b and S2).[28] This distortion together with the polar carboxylate–copper node provided the possibility to finely modify the electronic communication for the kinetic alleviation of fluorescence quenching of Cu(II) towards the highly reductive excited-state **TPA** moiety.[18]

In the absence of bulky auxiliary, a control catalyst was prepared by solvothermal reaction between $Cu(NO_3)_2$•$3H_2O$ and H_3**L-Planar** (45% yield). The (3,4)-connected three dimensional (3D) networks (internal diameter *ca*. 3.8 nm, Fig. S4) were assembled between the tritopic ligands and 4-connected $Cu_2(O_2C)_4$ paddle-wheels in a high-symmetry **tbo** topology (Table S1), similar to the well-known HKUST–1.[29] Notably, the absence of axial rotational restriction from the bulky auxiliary allowed the conformation of coplanar conjugation between the polar Cu(II)–carboxylate node and the adjacent phenyl moiety of ligand (Fig. 2c). Thus, this control coordination polymer was named as Cu–**Planar**. It should be noted that the existence or not of distortion along the axial direction of ligand did not affect the identical Cu–N_{TPA} distances (*ca*. 12.6 Å) in both Cu–**Twisted** and Cu–**Planar** (Figs. 2b and 2d), and the non-interpenetrated nature of two coordination polymers precluded the intermolecular luminescence quenching of Cu(II) nodes to the excited state of indirectly connected **TPA**-moieties. Moreover, the vast internal cavities and open windows of both Cu(II)-**TPA** coordination polymers were believed to facilitate the rapid mass transfer during their catalytic applications.

Electrochemical analyses of both Cu–**Twisted** and Cu–**Planar** exhibited the peaks at *ca*. 1.0 V corresponding to the redox potentials of the **TPA**-based ligands (Fig. S11). The similar reductive potentials of the excited-state frameworks were determined as -1.49 V and − 1.59 V for Cu–**Twisted** and Cu–**Planar**, respectively (Table S2), based on the free energy change (E^{0-0}) between the ground and vibrationally relaxed excited states (Fig. S12),[30] demonstrating that both the excited-state coordination polymers can theoretically reduce iodomesitylene dicyclohexanecarboxylate (abbreviated as $MesI(OCOCy)_2$, $E_{1/2}^{red}$ = -1.14 V *vs*. SCE), one of the prominent iodonium carboxylate-type radical precursors, for the generation of alkyl radicals.[7]

Electrochemical impedance spectroscopy (EIS) of the two coordination polymers exhibited different arc radii in the high-frequency regions, demonstrating that the charge-transfer resistance (R_{ct}) of Cu–**Twisted** (*ca*. 4.8 kΩ) was roughly three times larger than that of Cu–**Planar** (*ca*. 1.6 kΩ) (Fig. 3c). The photocurrent responses of two coordination polymers suggested their well reproducible photocurrents upon on/off cycles of the light irradiation (Fig. 3d). Compared with Cu–**Twisted**, a significant enhancement in the photocurrent response was observed for the case of Cu–**Planar**, indicating more efficient intramolecular PET process. Clearly, the twisted conjunction mode did not affect the thermodynamic photoreducing abilities of coordination polymers, but remarkably altered the kinetic features of intramolecular electronic communications.

The UV-Vis absorption spectra of solid-state Cu–**Twisted** and Cu–**Planar** exhibited the bands covering a broad visible range (400 ~ 550 nm, Fig. S10) that attributed to the absorption of **TPA**-based ligands, and the typical d-d transition peaks of dicopper paddle-wheel units were observed above 600 nm. As exhibited in Fig. 3a, upon photoirradiating the Cu–**Twisted** suspension in 1,4-dioxane, the obvious 536 nm-centred luminescence band indicated the weak intramolecular quenching of Cu(II) nodes towards the highly reductive excited-state **TPA** moieties. In comparison, the remarkably lower fluorescence intensity and shorter fluorescence lifetime (2.1 ns *vs*. 2.9 ns) of Cu–**Planar** suspension in 1,4-dioxane than those of Cu–**Twisted** under the identical conditions (Figs. 3a and 3b) suggested the more efficient intramolecular fluorescence quenching in the coordination polymer Cu–**Planar**.

Electron paramagnetic resonance (EPR) studies revealed that both coordination polymers exhibited the characteristic signals of Cu(II) ions with *g* value of *ca*. 2.09 (Fig. 5a).[31] Photoirradiation with compact fluorescent lamps for 15 min lead to significant depression of Cu(II) signal in EPR spectra of Cu–**Planar**. In comparison, the identical photoirradiation did not cause obvious Cu(II) signal variation in EPR spectra of Cu–**Twisted**, confirming that the twisted conjugation between **TPA**-moiety and polar carboxylate–copper node effectively hampered the intramolecular PET process between them (Figs. 2a and 2c). Moreover, the much greater amount of Cu(II) sites that retained in the photoirradiation of diode-like Cu–**Twisted** was believed to benefit the Cu(II) catalytic steps in its combination with photocatalysis (Fig. 1c).

Heterogeneous synergistic photoredox and copper catalysed decarboxylative C(sp^3)-heteroatom coupling. Noted that the carboxylic acids are more abundant, stable, and less toxic chemical feedstocks compared with alkyl halides, the classical alkyl radical precursor, thus the redox-activated carboxylic acids like iodonium carboxylates are considered as the practical and sustainable radical sources in this case. We next examined the synergistic photoredox and copper catalytic performances of the obtained Cu(II)–**TPA** coordination polymers using decarboxylative C(sp^3)-heteroatom coupling of iodonium carboxylates and heteroatom nucleophiles as the benchmark.[7] Upon addition of $MesI(OCOCy)_2$ into the suspensions of Cu–**Twisted** or Cu–**Planar** in 1,4-dioxane, the luminescences of coordination polymers were markedly quenched (Fig. S15). This result suggested a productive intermolecular PET from the excited state of **TPA** moiety to $MesI(OCOCy)_2$ was allowed for the generation of alkyl radicals. In a typical procedure, a mixture of $MesI(OCOCy)_2$, nitrogen-centred nucleophile 3-chloroindazole **2a**, basic additive

BTMG (BTMG = 2-*tert*-butyl-1,1,3,3-tetramethylguanidine), and 2.5 mol% Cu–**Twisted** in 1,4-dioxane was subjected to visible-light irradiation from a 405-nm LED under a N_2 atmosphere, and the desired C(sp^3)–N coupling product was obtained in 84% isolated yield after 5 hours (Fig. 4, 3a). Subsequently, a series of iodonium carboxylates derived from the primary linear, secondary acyclic and cyclic, and tertiary substituted alkyl carboxylic acids were found applicable in this protocol to deliver the corresponding *N*-alkyl heteroaryl products **3** in medium to good efficiencies (Fig. 4, 3a–3f). Especially, the use of tertiary carboxylic acid **3e** successfully introduced a sterically demanding adamantine moiety into the product in 86% yield; it should be noted that *N*-alkylation employing tertiary alkyl halides is elusive using traditional nucleophilic substitution. Interestingly, an ibuprofen derivative valuable to medicinal chemistry was accessible by this methodology (**3f**). In addition to indazole, other nitrogen heterocycles like indole, pyrrole, and phthalimide were also amenable to this *N*-alkylation protocol (**3 g**–**3i**). This catalytic system well tolerated functional groups such as terminal (**3c**) or internal (**3d**) olefins, which were inherently susceptible to radical addition, implying that Cu–**Twisted** might harness the behavior of radical species in an inner-spheric manner.

Control experiments demonstrated that coordination polymer catalyst and light irradiation were indispensable for the coupling reaction (Table S3, entries 2 and 3), neither the dark condition nor the absence of Cu–**Twisted** gave the formation of **3a**. There was no noticeable further conversion after hot filtration of Cu–**Twisted**, suggesting the heterogeneous nature of reaction (Table S3, entry 14). After photocatalysis, the coordination polymer was easily isolated from the reaction mixture by centrifugation and could be reused at least three times without a marked decrease in reactivity (83 ~ 79%; Fig. S25). The PXRD pattern of the recovered catalyst indicated that it maintained its structural integrity (Fig. S21). The nearly similar catalytic performances of the pristine crystals of coordination polymers compared to the finely ground samples ruled out the vital influence of particle sizes of heterogeneous catalysts towards catalytic efficacy (Fig. S22), implying that the reaction mainly occurred in the pores of coordination polymer (Table S3, entries 1, 4, 11 and 12).

When a radical scavenger tetramethylpiperidine-*N*-oxyl (TEMPO) was added to the reaction mixture, the conversion was inhibited immediately (Table S3, entry 13), suggesting a radical mechanism. The only use of ester form of ligand Et_3**L-Twisted** or Cu(II) salt as catalyst gave no reactions (Table S3, entries 7 and 9), reflecting the necessity of two kinds of catalytic sites. The simple combinations of Cu(II) salt either with Et_3**L-Twisted** or Me_3**L-Planar** afforded the low conversions, probably owing to the futile intermolecular fluorescence quenching of Cu(II) salt (Table S3, entries 5 and 6). The reference coordination polymer Cu–**Planar** gave a 41% yield of **3a**. Although this conversion was only half the level of Cu–**Twisted** (Table S3, entries 1 and 4), at least the incorporation of **TPA** moieties together with polar Cu(II)–carboxylate nodes into coordination polymer partially hampered the intermolecular fluorescence quenching that limited the direct combination of photoreductive dye and Cu(II) catalyst in the solution (Figs. 3a and 5a). Furthermore, if the similar redox potentials (Table S2), substrate encapsulating abilities, and intra-pore substrate diffusion kinetics (Fig. S24) of Cu–**Twisted** and Cu–**Planar** were also taken into

account, the distinct catalytic efficiencies of two coordination polymers (Fig. S23) might be attributed to their remarkably different intramolecular electronic communications.

The circular dichroism (CD) spectra of Cu–**Twisted** exhibited a negative signal at approximately 346 nm and positive dichroic band centered at 275 nm similar to that of H_3**L-Twisted** (Fig. S8), and the Cu(II) ions here were enveloped in the semi-open chiral pores (Fig. S2), which possibly provided stereoinduction in the radical capture of Cu(II) sites. When employing the iodonium carboxylate prepared from chiral natural derivative (1*R*,3*R*,4*S*)-*p*-menthane-3-carboxylic acid, the net resulting stereochemistry of the carboxylic *α*-carbon was fortunately maintained during C(sp^3)-N coupling (dr. > 20:1, Fig. 4, 3j) in the presence of proximal chiral centres on the menthane scaffold. After photoreductive decarboxylation, the frequent flipping of the formed C(sp^3)-centred radical erases the original stereoinformation,[32] thus it should be practical to use the radical precursors derived from the racemic α-substituted carboxylic acids. For **3 k** and **3 l**, chiralities were successfully introduced into the achiral *α*-positions of the carboxylic moieties by employing cheap racemic camphanic acid (**1 k**) and norbornene carboxylic acid (**1 l**) instead of their expensive enantioenriched homologs, demonstrating the inner-spheric redox process between the *in situ* generated radical species and the well-retained Cu(II)[33] within asymmetric local environment for controlling this diastereoselectivity.

Beside the iodonium carboxylates, the redox-active *N*-hydroxyphthalimide (NHPI) esters[34] derived from alkyl carboxylic acids were also the prominent alkyl radical precursors in decarboxylative cross-coupling reactions, as the surrogates for alkyl halides. Like that of iodonium carboxylate MesI$(OCOCy)_2$, the addition of NHPI ester **4c** into the Cu–**Twisted** suspension strongly quenched the luminescence (Figs. 5b and S16), whereas NHPI ester **4c** hardly quenched the fluorescence of Et_3**L**–**Twisted** (with a quite low quenching constant *K*sv < 0.01 $\mu mol^{-1} \cdot L$). As the excited-state reductive potential of Et_3**L-Twisted** was more negative than that of Cu–**Twisted** (Table S2), the Cu(II) sites of coordination polymer Cu–**Twisted** were speculated to improve the fluorescence quenching process of NHPI ester. IR spectra of Cu–**Twisted** crystals that soaked in the solution of NHPI ester **4c** exhibited the red-shifted carbonyl stretching peak of **4c** compared with that of the free molecule (Figs. 5c and S18), this potential interaction between the carbonyl of radical precursor **4c** and the Cu(II) site of coordination polymer might draw the radical precursor closer to the nearby photocatalytic centre,[35] which might be correlated to the above-mentioned enhancement of fluorescence quenching effect. Similarly, a bathochromic shift in the N–H stretching vibration of *ortho*-anisidine **5a** (3460 cm^{-1} to 3444 cm^{-1}) was also observed after substrate incubation within Cu–**Twisted**, verifying that the nitrogen atom of N–H was the nucleophilic binding site and could be activated during substrate adsorption within the coordination polymer (Figs. 5d and S19).

With minor changes of reaction conditions, this heterogeneous synergistic catalytic system was also applicable to the coupling of diverse primary, secondary, and tertiary alkyl redox-active NHPI esters with anilines in good yields (Fig. 6, 6a–6e).[36,37] Then, the substrate scope of this heterogeneous approach could be easily expanded from anilines to chalcogen-centred nucleophiles.[38] Phenols were successfully employed in C(sp^3)–O coupling (**6f**–**6 h**), and the *ortho*-phenylphenol fungicide derivative **6 h** was

obtained in 55% yield. Further extension of chalcogen-type nucleophiles to thiophenols facilitated rapid access to thioether-derived Naproxen **6 l**, showcasing the efficient late-stage functionalisation for drugs and the perfect resistance to the potential sulphur-poisoning effect.

As shown in Fig. 7, our heterogeneous synergistic catalytic strategy using a twisted-conjugated Cu(II)–dye coordination polymer supplies a unified mechanistic paradigm to meet the diversified needs of reaction kinetics between photoredox and copper catalytic cycles[3] when employing the different types of substrates and radical precursors. Upon light irradiation, the diode-like coordination polymer Cu–**Twisted** hampers the intramolecular fluorescence quenching to switch on the intermolecular PET from the excited-state **TPA** moiety of ligand to the alkyl radical precursor that possibly activated by the Cu(II) site. The *in situ* generated alkyl radical is subjected to an inner-spheric redox process with the Cu(II) site that coordinates with the heteroatom-centred nucleophile, delivering Cu(I) species and the desired coupling product, as depicted by the pioneering homogeneous protocols.[39] Then, the radical cation of the oxidized **TPA** moiety retrieves one electron from the Cu(I) site through the twisted connection at the ground state, which completes the productive closed-circuit electron transfer route for the synergy of photocatalytic and copper catalytic cycles and simultaneously regenerates the resting-state Cu–**Twisted** for the next round of reaction.[14] Within the confined environments of Cu–**Twisted**, the well-retained Cu(II) sites enriches substrates and reagents to improve the local concentration of activated nucleophiles and *in situ* generated alkyl radicals. This key kinetic modulation is believed to furnish the heterogeneous synergistic photoredox and copper catalysis in a concise and easy handling manner, which alleviates the reliance on the varied and elaborative reaction conditions obtained by the massive screening efforts that typically needed in the homogeneous protocols when using different types of nucleophiles and radical precursors. In a comparison, the low concentration of the transient Cu(II) species that *in situ* generated from the homogeneous Cu(I)-photocatalyst system might hamper them from exerting the readily accessible modulation effects.[3,40]

Heterogeneous synergistic photoredox and copper catalysed trifluoromethylation-chloration difunctionalisation. As mentioned above, the well-retained Cu(II) centres during PET process enabled the inner-spheric capture of single-electronic radical intermediates and the fixation of double-electronic heteroatom-centred nucleophiles and carbonyl-containing radical precursors, which shed light on different-typed value-added catalytic application by integrating nucleophiles, carbonyl-containing substrates, and radical species in a step-economic manner, such as the pharmaceutically important trifluoromethylation-chloration difunctionalisation[41] of olefins of α,β-unsaturated compounds. Appending CF_3 and Cl moieties to olefins was highly dependent on the copper-mediated inner-spheric processes,[42,43] since that the olefinic moieties were prone to either the intermolecular radical oligomerisation/polymerisation or the intramolecular cyclisation when encountered with free radicals. The negative enough reductive potential of excited-state Cu–**Twisted** allowed the photoreduction of triflyl chloride (TfCl) ($E_{1/2}^{red}$ = -0.18 V vs. SCE),[44] the typical CF_3 radical precursor. As a consequence, the quenching of 512-nm luminescence of the acetonitrile suspension of Cu–**Twisted** crystals upon the

addition of TfCl was indicative of the PET process from excited-state **TPA**-based ligand to TfCl for the generation of CF_3 radicals under light irradiation (Fig. S17).

Given the propensity of the methacrylate ester to undergo the radical oligomerisation/polymerisation,[45] the phenyl methacrylate (Fig. 8a, 7a) was chosen as the model substrate of difunctionalisation by Cu–**Twisted**. In a typical procedure, a mixture of phenyl methacrylate **7a**, TfCl, basic additive (2,4,6-collidine), and 2.5 mol% Cu–**Twisted** in acetonitrile was subjected to visible-light irradiation from two household compact fluorescent lamps (CFLs), obtaining the trifluoromethylation-chloration product **8a** in an isolated yield of 92% (Fig. 8a), and no radical oligomerisation/polymerisation products could be detected. The only use of Et_3**L- Twisted** resulted in the dominative oligomerisation/polymerisation of the substrate (Table S5, entry 7), and the simple combination of Cu(II) salt and Et_3**L-Twisted** gave a hugely diminished conversion (13%), reflecting the necessity of the *holo* coordination polymer for hampering the undesirable intermolecular fluorescence quenching (Table S5, entry 9). When using the controlled catalyst Cu–**Planar**, a lower yield of 45% was detected, implying the importance of well-rectified intramolecular electronic communication in the diode-like catalyst for the efficient diffunctionalisation (Table S5, entry 4). Furthermore, various *α,β*-unsaturated esters (**7b** to **7e**) were transformed to the corresponding *α*-chloro-*β*-trifluoromethyl ester products in good to high yields. Besides, the *α,β*-unsaturated amides (**7f** to **7 h**) also participated well in this difunctionalisation, and the well-known radical cyclisations with intramolecular *N*-phenyl moieties were effectively depressed (see also Fig. S28).[46] Those results indicated that the carbon-centred radical intermediates formed after CF_3 radical addition might be intercepted by the Cu(II) nodes to prohibit the side-pathways like oligomerisation/polymerization or cyclisation. Attaching bulky auxiliaries to the neighbouring positions of carbonyl groups of the substrates should benefit the mutual stereo-recognition and induction between substrates and local environments (**7i** to **7 k**). In particular, the reaction of **7 k** bearing a bio-relevant dihydrocholesterol fragment, afforded the targeted product nearly as sole diastereomer (Fig. 8a, 8 k).

Structurally complex small molecules containing repeating functional groups,[47] like multiple olefinic natural products, have an extraordinary capacity for a wide range of useful functions.[48] The similar thermodynamic reactivities of different olefinic sites of natural derivatives made the discrimination of olefinic groups a challenging task in the presence of highly active CF_3 radicals, like in the case of trifluoromethylation-chloration difunctionalisation (Table S6).[49] Here, the natural flavour derivative **7 l** containing a carbonyl-adjacent olefin and a carbonyl-free olefin in the molecular scaffold was chosen as the model substrate.[50] DFT calculation revealed the thermodynamic feasibility of docking the carbonyl site of substrate **7 l** through Cu–O interaction (Table S7), with a free energy change of *ca*. 12.44 kcal•mol^{-1} in **7 l** over the adsorption upon Cu(II) node. The IR spectra of Cu–**Twisted** with encapsulated **7 l** suggested that the C = O stretching peak of **7 l** was red-shifted relative to that of the free molecule (1744 to 1732 cm^{-1}, Fig. S20), verifying the possible fixation of the carbonyl moiety of substrate on the Cu(II) site. As a consequence, the distances between the multiple olefinic sites of the docked substrate

and the catalytic centres should be effectively differentiated within Cu–**Twisted**, which might provide an ideal model of the Hammond postulate-typed site-selectivity control (Fig. S30).[51]

Under the typical reaction conditions of Fig. 8a, the trifluoromethylation-chloration difunctionalisation of **7 l** solely occurred on the carbonyl-adjacent olefinic site and afforded the formation of product **8 l** in an isolated yield of 71% (Fig. 8b), and the carbonyl free olefinic site of allylbenzene terminal of **7 l** was well retained. To the contrast, the olefinic site of the free standing control substrate allylbenzene well participated in the difunctionalisation under the identical catalytic condition (Fig. S29).[43] It was deduced that the spatial proximity between the **TPA** moiety and the docked carbonyl of substrate might facilitate the formation of a product-like late transition state[52] by restricting the photogenerated CF_3 radical near to the fixed α,β-unsaturated olefinic group in the confined space, which might be important to kinetically distinguish the bonded and unbonded olefinic sites within the same molecules (Fig. S30). When the biologically interesting steride scaffolds containing olefinic sites were merged together with the α,β-unsaturated esters, the corresponding steride derivatives **7p** and **7q** delivered excellent regio- and diastereocontrol simultaneously, and the carbonyl-adjacent olefinic terminals of substrates were converted with perfect diastereoselectivity while retaining single or even multiple carbonyl-free alkenes in the fragments of cholesterol and ergosterol (Fig. 8b, 8p and 8q), illustrating the potential of this heterogeneous synergistic photoredox-copper catalytic system in drug discovery.

Then, DFT calculations were performed to investigate the role of readily accessible Cu(II) sites of Cu–**Twisted** in discriminating different olefinic sites during the synergistic catalytic difunctionalisation. As shown in Fig. 9, the computed energy profiles of the reaction pathways of the carbonyl-adjacent olefinic site (pathway **a**, in red) of **7 l** and the opposite-side carbonyl-free allyl terminal (pathway **b**, in blue) were compared. Addition of the CF_3 radical to the olefinic site nearby the docked carbonyl **7 l** occurs *via* transition state **TS I** by an energy barrier of 16.76 kcal•mol^{-1} to form carbon-centred radical intermediate **II**. Subsequently, the chloride anion coordinates to the copper centre and replaces the carbonyl moiety, and the copper–Cl species mediates Cl-atom transfer to form **8 l**.[53] The overall transformation *via* pathway **a** is exergonic by 12.19 kcal•mol^{-1}. In contrast, addition of the CF_3 radical to the carbonyl-free allyl terminal of **7 l** occurs through transition state **TS I'** with a higher energy barrier of 25.6 kcal•mol^{-1}, and all subsequent steps also proceed through higher energy barriers despite pathway **b** being more thermodynamically favourable overall (exergonic by 24.21 kcal•mol^{-1}).

Consequently, the two thermodynamically allowed pathways were distinguished within coordination polymer, and the difunctionalisation of olefinic moiety that adjacent to carbonyl binding site in the same molecules was kinetically favoured (Fig. 8b and Table S6). Moreover, it was revealed that the adsorption of substrate **7 l** was more favoured than that of product **8 l** (the comparison of DFT calculated free energy changes, -12.44 < -11.03 kcal·mol^{-1}, see Table S7). This result implied that the generated product may be crowded out from Cu(II) centre by the competitive adsorption of a substrate molecule to trigger the new round of reaction, facilitating the recyclability of the heterogeneous catalysts.

Discussion

In summary, we have developed a novel heterogeneous approach to combining photoredox and copper catalysis for decarboxylative C(sp^3)-heteroatom couplings and site-selective trifluoromethylation difunctionalisation of olefins by using Cu(II)–dye coordination polymer. The twisted conjugation between photoreductive **TPA**-moiety and the polar carboxylate–Cu(II) node in coordination polymer featured the photoelectronic behavior of molecular diode array for hampering the futile inter- and intramolecular fluorescence quenching of Cu(II) site towards **TPA**-based ligand, rectifying the productive unidirectional electron transfer route. Thus, the high local concentration of Cu(II) sites that retained during PET process exerted the unique modulation effects on substrates, reagents, and radical intermediates, endowing the synergistic photoredox and copper catalysis with the much broader adaptability to different types of value-added reactions, the concise and easy handling reaction conditions, and the distinctive reaction selectivities. Fabrication of the coordination polymer employs economic organic dyes in place of noble-metal-complex photosensitisers, and the heterogeneity of the reactions facilitates catalyst recovery after use, circumventing the residual heavy metal issues of usual homogeneous protocols. This package deal paves the way for designing novel synergistic photoredox and high-valent transition-metal catalytic systems from an intrinsic perspective of molecular device, which might trigger tremendous new possibilities in both fields of pharmaceuticals and photoelectronics.

Methods

Materials and measurements. All commercial chemical sources and experimental details for ^{1}H NMR, ^{13}C NMR, ^{19}F NMR, HRMS, IR, thermogravimetric analysis, EPR, CV, EIS, single-crystal X-ray crystallography, PXRD, and photoelectrochemical measurements are provided in the Supplementary Material.

Synthesis of Cu–Twisted. A mixture of H_3**L-Twisted** (0.02 mmol) and $Cu(NO_3)_2 \cdot 3H_2O$ (0.08 mmol) were dissolved into solvent mixture of DMF/MeOH (3 mL/1 mL), in a vial. After addition of 3 drops of HCl (3 M, aq.), the vial was sealed in a Teflon-lined stainless steel autoclave and heated at 80 °C for 3 days. The reaction system was then cooled to room temperature at a rate of 5 °C h^{-1}. Green block crystals were collected in 70% yield (based on ligand). Elememt analysis (%) calc. for $C_{198}H_{204}N_{14}O_{51}Cu_3$: H, 5.43; C, 62.81; N, 5.18%. Found: H, 5.58; C, 62.76; N, 5.09%. IR (KBr): 3390, 2962, 1729, 1597, 1517, 1489, 1438, 1386, 1323, 1262, 1214, 1189, 1148, 1051, 1015, 969, 859, 830, 766, 729, 681, 654, 521 cm^{-1}. ^{1}H NMR (400 MHz, DMSO-d_6/DCl): δ = 7.97 (d, J = 8.2 Hz, 3H), 7.77 (d, J = 8.7 Hz, 6H), 7.74 (dd, J = 8.5 and 1.6 Hz, 3H), 7.65 (d, J = 1.3 Hz, 3H), 7.24 (d, J = 8.6 Hz, 6H), 4.49–4.39 (m, 6H), 4.26 (dd, J = 6.8 and 4.8 Hz, 3H), 1.97–1.91 (m, 3H), 0.94 (d, J = 6.8 Hz, 9H), 0.82 (d, J = 6.9 Hz, 9H).

Typical procedure for decarboxylative C(sp^3)-N coupling of iodonium carboxylates. To a pre-dried Pyrex tube equipped with a cooling water system was added specified amounts of catalyst (2.5 mol%, 7.5 μmol), *N*-nucleophile (1 equiv., 0.30 mmol), and hypervalent iodine (2 equiv., 0.60 mmol, prepared according to the literature protocol[7]), then the tube was sealed and subjected to three vacuum/N_2 refill

cycles. After adding anhydrous degassed 1,4-dioxane (6 mL) and base BTMG (2 equiv., 0.60 mmol) by syringe, the reaction mixture was stirred and irradiated with 405-nm LEDs for 5 h. The catalyst was filtered, the filtrate was concentrated under reduced pressure, and the product was isolated via flash chromatography on silica gel.

Typical procedure for decarboxylative C(sp^3)-heteroatom coupling of redox-active esters. To a pre-dried Pyrex tube equipped with a cooling water system was added specified amounts of catalyst (2.5 mol%, 7.5 μmol), nucleophile (1.0 equiv., 0.30 mmol), and redox-active NHPI ester (2.0 equiv., 0.60 mmol), then the tube was sealed and subjected to three vacuum/N_2 refill cycles. After adding anhydrous degassed MeCN (3 mL) and base DIPEA (*N*,*N*-diisopropylethylamine, 3.0 equiv., 0.90 mmol) by syringe, the reaction mixture was stirred and irradiated with 405-nm LEDs for 12 h. The catalyst was filtered, the filtrate was concentrated under reduced pressure, and the product was isolated via flash chromatography on silica gel.

Typical procedure for trifluoromethylation-chloration difunctionalisation of olefins. To a pre-dried Pyrex tube equipped with a cooling water system was added specified amounts of catalyst (2.5 mol%, 6.25 μmol) and substrate (1.0 equiv., 0.25 mmol), then the tube was sealed and subjected to three vacuum/N_2 refill cycles. After adding anhydrous degassed MeCN (1 mL), base 2,4,6-collidine (2.5 equiv., 0.625 mmol), and TfCl (2.5 equiv., 0.625 mmol) by syringe, the reaction mixture was stirred and irradiated with visible light by two 20-W household CFLs for 12 h. The catalyst was filtered, the filtrate was concentrated under reduced pressure, and the product was isolated via flash chromatography on silica gel.

Data availability

The X-ray crystallographic coordinates for the structures reported in this article have been deposited at the Cambridge Crystallographic Data Centre (CCDC) under the deposition number CCDC 1870816 (Table S1). These data can be obtained free of charge from The Cambridge Crystallographic Data Centre via www.ccdc.cam.ac.uk/data_request/cif. All other data supporting the findings of this study are available within the article and its Supplementary Information files or from the corresponding author upon request.

Declarations

Acknowledgements

This work was supported by the National Natural Science Foundation of China (21971031, 21890381, and U1608224).

Author Contributions

Y. S. and T. Z. contributed equally to this work. T. Z. and C. D. conceived the project, designed the experiments, and wrote the manuscript. Y. S. and T. Z. performed the experiments. X.-M. J. and G. X.

analysed and refined the powder X-ray diffraction data. Y. S., C. H., and C. D. solved and refined the X-ray crystal structures. All authors discussed the results and commented on the manuscript.

Additional information

Supplementary Information is available in the online version of the paper. Correspondence and requests for materials should be addressed to C. D. (Email: cyduan@dlut.edu.cn).

Competing interests: The authors declare no competing financial interests.

Reprints and permission information is available online at http://npg.nature.com/reprintsandpermissions/

References

1. Ruiz-Castillo, P. & Buchwald, S. L. Applications of palladium-catalyzed C–N cross-coupling reactions. *Chem. Rev.* **116**, 12564–12649 (2016).
2. Tran, B. L., Li, B., Driess, M. & Hartwig, J. F. Copper-catalyzed intermolecular amidation and imidation of unactivated alkanes. *J. Am. Chem. Soc.* **136**, 2555–2563 (2014).
3. Hossain, A., Bhattacharyya, A. & Reiser, O. Copper's rapid ascent in visible-light photoredox catalysis. *Science* **364**, eaav9713 (2019).
4. Greaney, M. F. Copper catalysis in a blue light. *Science* **351**, 666 (2016).
5. Demas, J. N. & Addington J. W. Luminescence quenching of dicyanobis (1,10-phenanthroline) ruthenium (II) by cupric ion in aqueous solutions. Dynamic and static processes. *J. Am. Chem. Soc.* **96**, 3663–3664 (1974).
6. Ye, Y. & Sanford, M. S. Merging visible-light photocatalysis and transition-metal catalysis in the copper-catalyzed trifluoromethylation of boronic acids with CF_3I. *J. Am. Chem. Soc.* **134**, 9034–9037 (2012).
7. Liang, Y., Zhang, X., MacMillan, D. W. C. Decarboxylative sp^3 C-N coupling via dual copper and photoredox catalysis. *Nature* **559**, 83–88 (2018).
8. Bao, X., Wang, Q., Zhu, J. Dual photoredox/copper catalysis for the remote C(sp^3)-H functionalization of alcohols and alkyl halides by *N*-alkoxypyridinium salts. *Angew. Chem. Int. Ed.* **58**, 2139–2143 (2019).
9. Zeng, L. *et al*. Photoactivation of Cu centers in metal – organic frameworks for selective CO_2 conversion to ethanol. *J. Am. Chem. Soc.* **142**, 75–79 (2020).
10. Feng, X.; Pi, Y.; Song, Y.; Brzezinski, C.; Xu, Z.; Li, Z.; Lin, W. Metal – Organic Frameworks Significantly Enhance Photocatalytic Hydrogen Evolution and CO_2 Reduction with Earth-Abundant Copper Photosensitizers. *J. Am. Chem. Soc.* **142**, 690–695 (2020).

11. Zhu, Y.-Y. et.al. Merging Photoredox and Organometallic Catalysts in a Metal–Organic Framework Significantly Boosts Photocatalytic Activities. *Angew. Chem.* **130**, 14286–14290 (2018).
12. Kim, D., Whang, D. R. & Park, S. Y. Self-healing of molecular catalyst and photosensitizer on metal–organic framework: robust molecular system for photocatalytic H_2 evolution from water. *J. Am. Chem. Soc.* **138**, 8698–8701 (2016).
13. Wu, P. *et al*. Luminescent metal-organic frameworks for selectively sensing nitric oxide in an aqueous solution and in living cells. *Adv. Funct. Mater.* **22**, 1698–1703 (2012).
14. Grabowski, Z. R., Rotkiewicz, K., Rettig, W. Structural Changes Accompanying Intramolecular Electron Transfer: Focus on Twisted Intramolecular Charge-Transfer States and Structures. *Chem. Rev.* **103**, 3899–4032 (2003).
15. Venkataraman, L., Klare, J. E., Nuckolls, C., Hybertsen, M. S. & Steigerwald, M. L. Dependence of single-molecule junction conductance on molecular conformation. *Nature* **442**, 904–907 (2006).
16. Van Wyk, A., Smith, T, Park, J. & Deria, P. Charge-transfer within Zr-based metal–organic framework: the role of polar node. *J. Am. Chem. Soc.* **140**, 2756–2760 (2018).
17. Zhang, T., Guo, X., Shi, Y., He, C. & Duan, C. Dye-incorporated coordination polymers for direct photocatalytic trifluoromethylation of aromatics at metabolically susceptible positions. *Nat. Commun.* **9**, 4024 (2018).
18. Janes, D. Molecular electronics: rectifying current behaviours. *Nat. Chem.* **1**, 601–603 (2009).
19. Shustova, N. B., McCarthy, B. D. & Dinca, M. Turn-on fluorescence in tetraphenylethylene-based metal–organic frameworks: an alternative to aggregation-induced emission. *J. Am. Chem. Soc.* **133**, 20126–20129 (2011).
20. Chisholm, M. H., Feil, F., Hadad, C. M. & Patmore, N. J. Electronically Coupled MM Quadruply-Bonded Complexes (M = Mo or W) Employing Functionalized Terephthalate Bridges: Toward Molecular Rheostats and Switches. *J. Am. Chem. Soc.* **127**, 18150–18158 (2005).
21. Li, J. J., Johnson, D. S., Sliskovic, D. R. & Roth, B. D. Contemporary drug synthesis, (*Wiley*, *Hoboken*, 2004).
22. Müller, K., Faeh, C. & Diederich, F. Fluorine in pharmaceuticals: looking beyond intuition. *Science* **317**, 1881–1886 (2007).
23. Vitaku, E., Smith, D. T. & Njardarson, J. T. Analysis of the structural diversity, substitution patterns, and frequency of nitrogen heterocycles among U.S. FDA approved pharmaceuticals. *J. Med. Chem.* **57**, 10257–10274 (2014).
24. Gedrich, K. *et al*. A family of chiral metal–organic frameworks. *Chem. Eur. J.* **17**, 2099–2106 (2011).
25. Le Bail, A., Duroy, H. & Fourquet J. L. Ab-initio structure determination of $LiSbWO_6$ by X-ray powder diffraction. *Mater. Res. Bull.* **23**, 447–452 (1988).
26. Ma, L., Falkowski, J. M., Abney, C. & Lin, W. *Nat. Chem.* **2**, 838–846 (2010).
27. Braun, M. E., Steffek, C. D., Kim, J., Rasmussen P. G. & Yaghi, O. M. 1,4-Benzenedicarboxylate derivatives as links in the design of paddle-wheel units and metal–organic frameworks. *Chem.*

Commun. 2532–2533 (2001).

28. Lu, W. *et al*. Tuning the structure and function of metal–organic frameworks via linker design. *Chem. Soc. Rev.* **43**, 5561–5593 (2014).
29. Chui, S. S.-Y., Lo, S. M.-F., Charmant, J. P. H., Orpen, A. G. & Williams, I. D. A chemically functionalizable nanoporous material $[Cu_3(TMA)_2(H_2O)_3]_n$. *Science* **283**, 1148–1150 (1999).
30. Kavarnos, G. J. Fundamentals of photoinduced electron transfer, (*Wiley*, *New York*, 1993).
31. Pöppl, A., Kunz, S., Himsl, D. & Hartmann, M. CW and pulsed ESR spectroscopy of cupric ions in the metal – organic framework compound $Cu_3(BTC)_2$. *J. Phys. Chem. C* **112**, 2678–2684 (2008).
32. Yan, M., Lo, J. C., Edwards, J. T. & Baran, P. S. Radicals: reactive intermediates with translational potential. *J. Am. Chem. Soc.* **138**, 12692–12714 (2016).
33. Kainz, Q. M. *et al*. Asymmetric copper-catalyzed C–N cross-couplings induced by visible light. *Science* **351**, 681–684 (2016).
34. Murarka, S. *N*-(acyloxy)phthalimides as redox-active esters in cross-coupling reactions. *Adv. Synth. Catal.* **360**, 1735–1753 (2018).
35. Hendon, C. H. & Walsh, A. Chemical principles underpinning the performance of the metal–organic framework HKUST-1. *Chem. Sci.* **6**, 3674–3683 (2015).
36. Mao, R., Frey, A., Balon, J. & Hu, X. Decarboxylative C(sp^3)-N cross-coupling via synergetic photoredox and copper catalysis. *Nat. Catal.* **1**, 120–126 (2018).
37. Zhao, W., Wurz, R. P., Peters, J. C. & Fu, G. C. Photoinduced, copper-catalyzed decarboxylative C–N coupling to generate protected amines: an alternative to the Curtius rearrangement. *J. Am. Chem. Soc.* **139**, 12153–12156 (2017).
38. Mao, R., Balon, J. & Hu, X. Decarboxylative C(sp^3)-O cross-coupling. *Angew. Chem. Int. Ed.* **57**, 13624–13628 (2018).
39. Zhao, X., Liu, Y., Zhu, R., Liu, C. & Zhang, D. Mechanistic Study on the Decarboxylative sp^3 C–N Cross-Coupling between Alkyl Carboxylic Acids and Nitrogen Nucleophiles via Dual Copper and Photoredox Catalysis. *Inorg. Chem.* **58**, 12669–12677 (2019).
40. Iwamura, M., Takeuchi, S. & Tahara, T. Ultrafast excited-state dynamics of copper(I) complexes. *Acc. Chem. Res.* **48**, 782–791 (2015).
41. Egami, H.; Sodeoka, M. Trifluoromethylation of Alkenes With Concomitant Introduction of Additional Functional Groups. *Angew. Chem. Int. Ed.* **53**, 8294–8308 (2014).
42. Tang, X.-J.; Dolbier, W. R., Jr. Efficient Cu-Catalyzed Atom Transfer Radical Addition Reactions of Fluoroalkylsulfonyl Chlorides with Electron-Deficient Alkenes Induced by Visible Light. *Angew. Chem. Int. Ed.* **54**, 4246–4249 (2015).
43. Bagal, D. B.; Kachkovskyi, G.; Reiser, O. Trifluoromethylchlorosulfonylation of Alkenes: Evidence for an Inner-Sphere Mechanism by a Copper Phenanthroline Photoredox Catalyst. *Angew. Chem. Int. Ed.* **54**, 6999–7002 (2015).

44. Nagib, D. A. & MacMillan, D. W. C. Trifluoromethylation of arenes and heteroarenes by means of photoredox catalysis. *Nature* **480**, 224–228 (2011).
45. Theriot, J. C. et al. Organocatalyzed atom transfer radical polymerization driven by visible light. *Science* **352**, 1082 – 1086 (2016).
46. Tang, X.-J.; Thomoson, C. S.; Dolbier, W. R., Jr. Photoredox-Catalyzed Tandem Radical Cyclization of *N*-Arylacrylamides: General Methods to Construct Fluorinated 3,3-Disubstituted 2-Oxindoles Using Fluoroalkylsulfonyl Chlorides. *Org. Lett.* **16**, 4594–4597 (2014).
47. Snyder, S. A., Gollner, A. & Chiriac, M. I. Regioselective reactions for programmable resveratrol oligomer synthesis. *Nature* **474**, 461–466 (2011).
48. Huang, Z. & Dong, G. Site-selectivity control in organic reactions: a quest to differentiate reactivity among the same kind of functional groups. *Acc. Chem. Res.* **50**, 465–471 (2017).
49. Low, H. C., Tedder, J. M. & Walton, J. C. Free radical addition to olefins. Part 19.-Trifluoromethyl radical addition to fluoro-substituted propenes and its absolute rate of addition to ethylene. *J. Chem. Soc., Faraday Trans. 1: Phys. Chem. Condens. Phases* **72**, 1300–1309 (1976).
50. Baser, K. H. C.; Tabanca, N.; Kirimer, N.; Bedir, E.; Khan, I. A.; Wedge, D. E. Recent Advances in the Chemistry and Biological Activities of the Pimpinella Species of Turkey. Recent Advances in the Chemistry and Biological Activities of the Pimpinella Species of Turkey. *Pure Appl. Chem.* **79**, 539–556 (2007).
51. Wilcock, B. C., Uno, B. E., Bromann, G. L., Clark, M. J., Anderson, T. M. & Burke, M. D. Electronic tuning of site-selectivity. *Nat. Chem.* **4**, 996–1003 (2012).
52. Lichtor, P. A. & Miller, S. J. Combinatorial evolution of site- and enantioselective catalysts for polyene epoxidation. *Nat. Chem.* **4**, 990–995 (2012).
53. Liu, Z. et al. Radical carbofluorination of unactivated alkenes with fluoride ions. *J. Am. Chem. Soc.* **140**, 6169–6175 (2018).

Figures

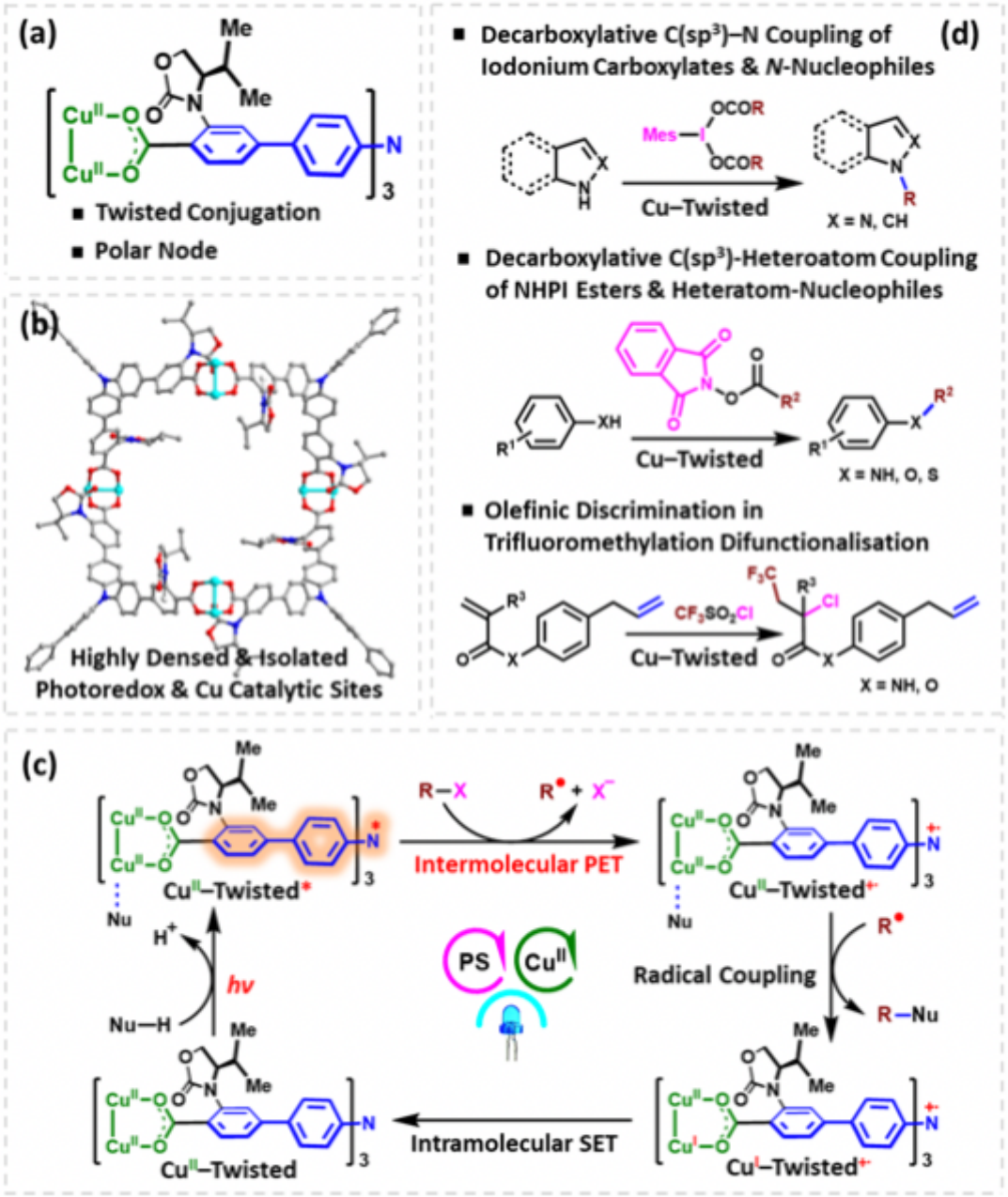

Figure 1

Diode-like Cu(II)–dye rectifier within coordination polymer for synergistic photoredox and copper catalysis. a, Schematic illustrations of the twisted conjugation between polar Cu(II)-carboxylate node and photoreductive TPA-moiety with bulky oxazolidinone auxiliaries; b, the densed fixation and spatial isolation of photoredox and Cu(II) catalytic sites in coordination polymer; c, the mechanistic perspective of synergistic photoredox and copper catalysis by the diode-like Cu(II)–dye coordination polymer for the typical couplings; d, heterogeneous catalytic application of Cu(II)–dye coordination polymer in decarboxylative C(sp3)-heteroatom couplings and site-selective trifluoromethylation difunctionalisation of olefins.

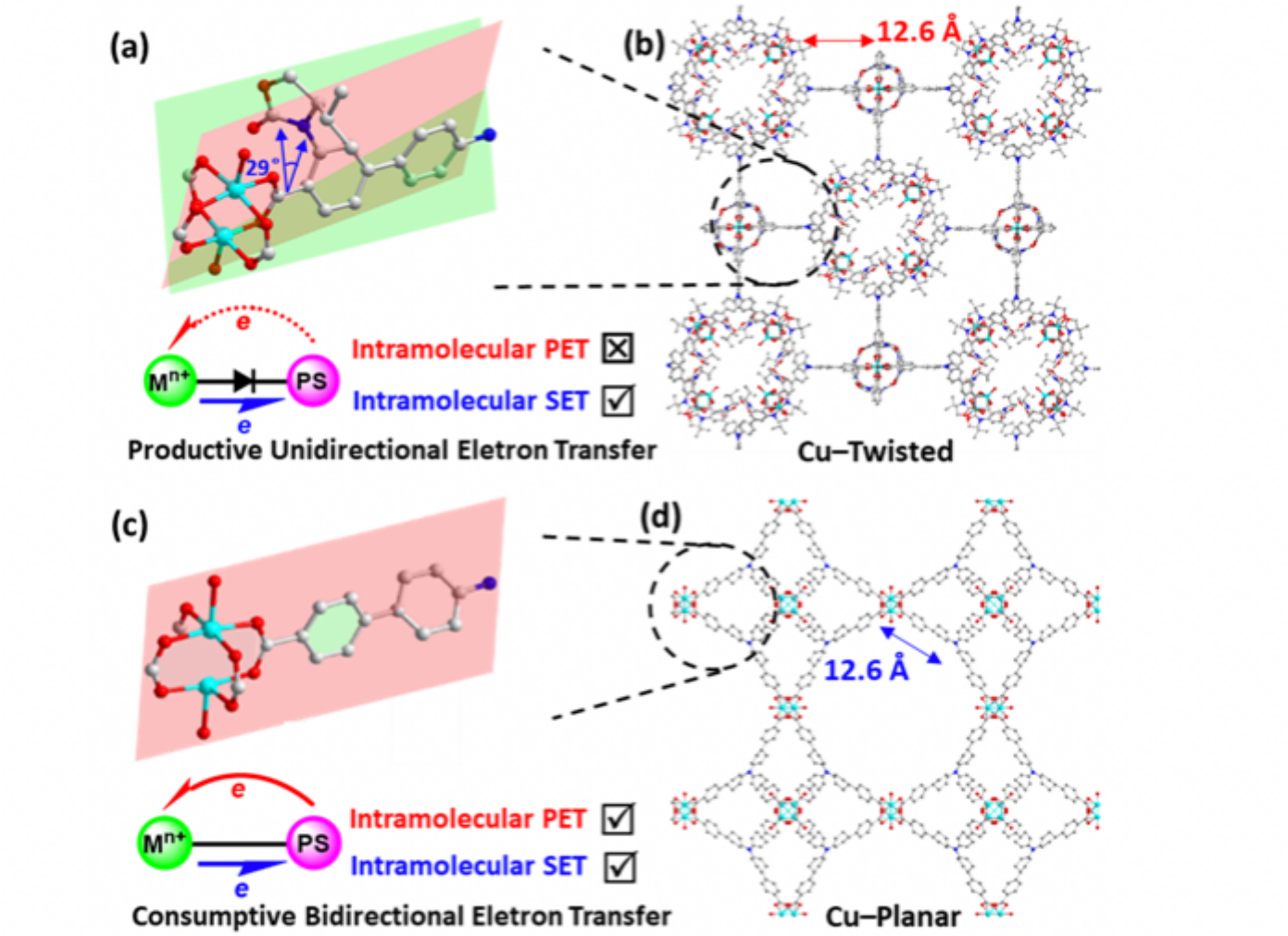

Figure 2

Cu(II)–TPA coordination polymers with and without twisted conjugation. a, The twisted dihedral angle between Cu(II)–carboxylate coordination plane and neighbouring phenyl plane of Cu–Twisted. The inset exhibited the possible diode-like unidirectional intramolecular electron transfer route in Cu–Twisted. b, The 3D porous network of Cu–Twisted. c, The coplanar conjugation between Cu(II)–carboxylate coordination plane and neighbouring phenyl plane of Cu–Planar. The inset exhibited the potential molecular wire-like bidirectional intramolecular electron transfer route in Cu–Planar. d, The 3D porous network of Cu–Planar. Cu, cyan; C, grey; O, red; N, blue; H atoms were omitted for clarity.

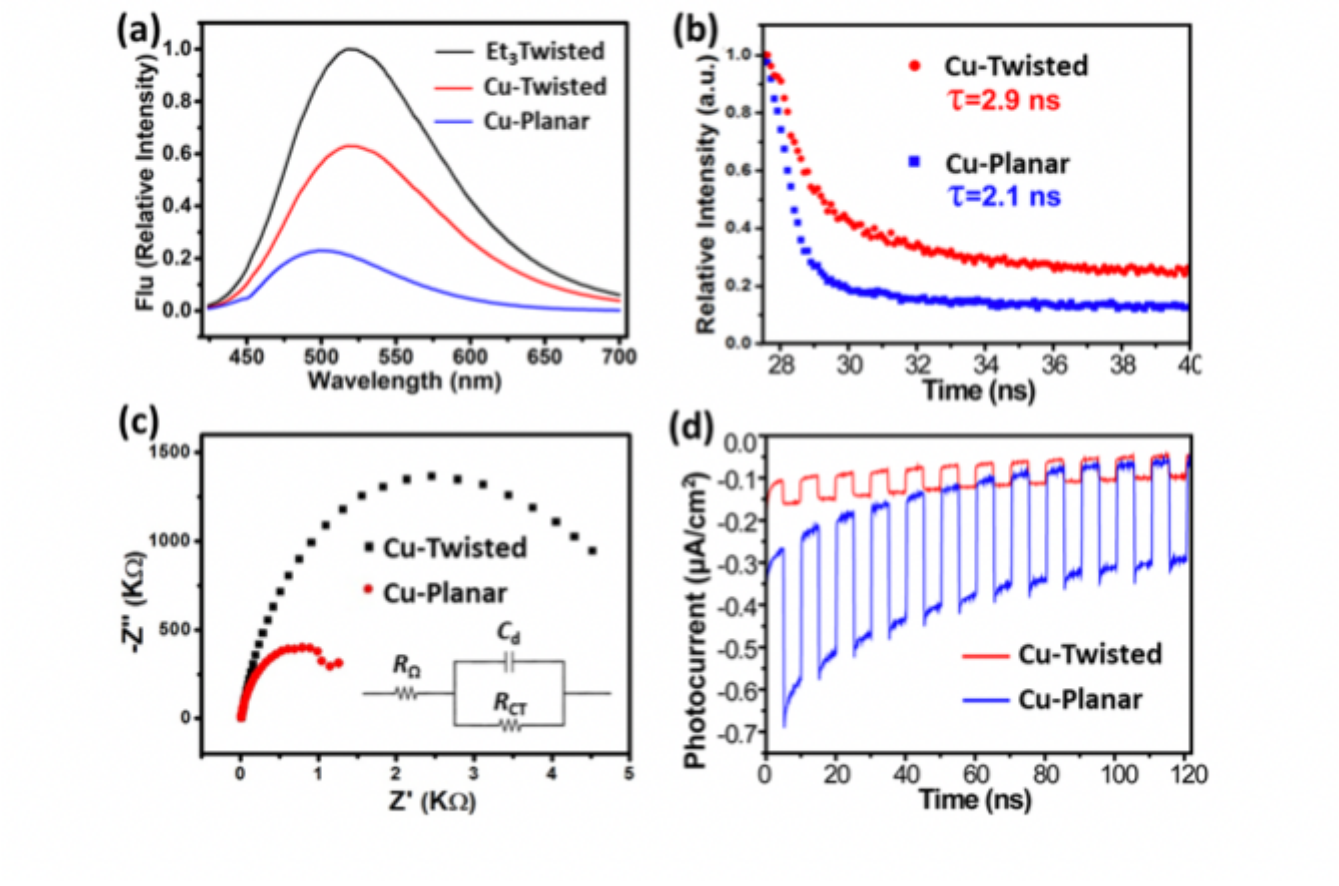

Figure 3

Characterisation of the diode-like photoelectronic behaviours of Cu(II)–TPA coordination polymers. a, Comparative illustration of fluorescence of Cu–Twisted, Cu–Planar, and ester form of ligand. Comparisons of b fluorescence lifetimes, c electrochemical impedance spectra (EIS), and d transient photocurrent responses of Cu–Twisted and Cu–Planar, respectively.

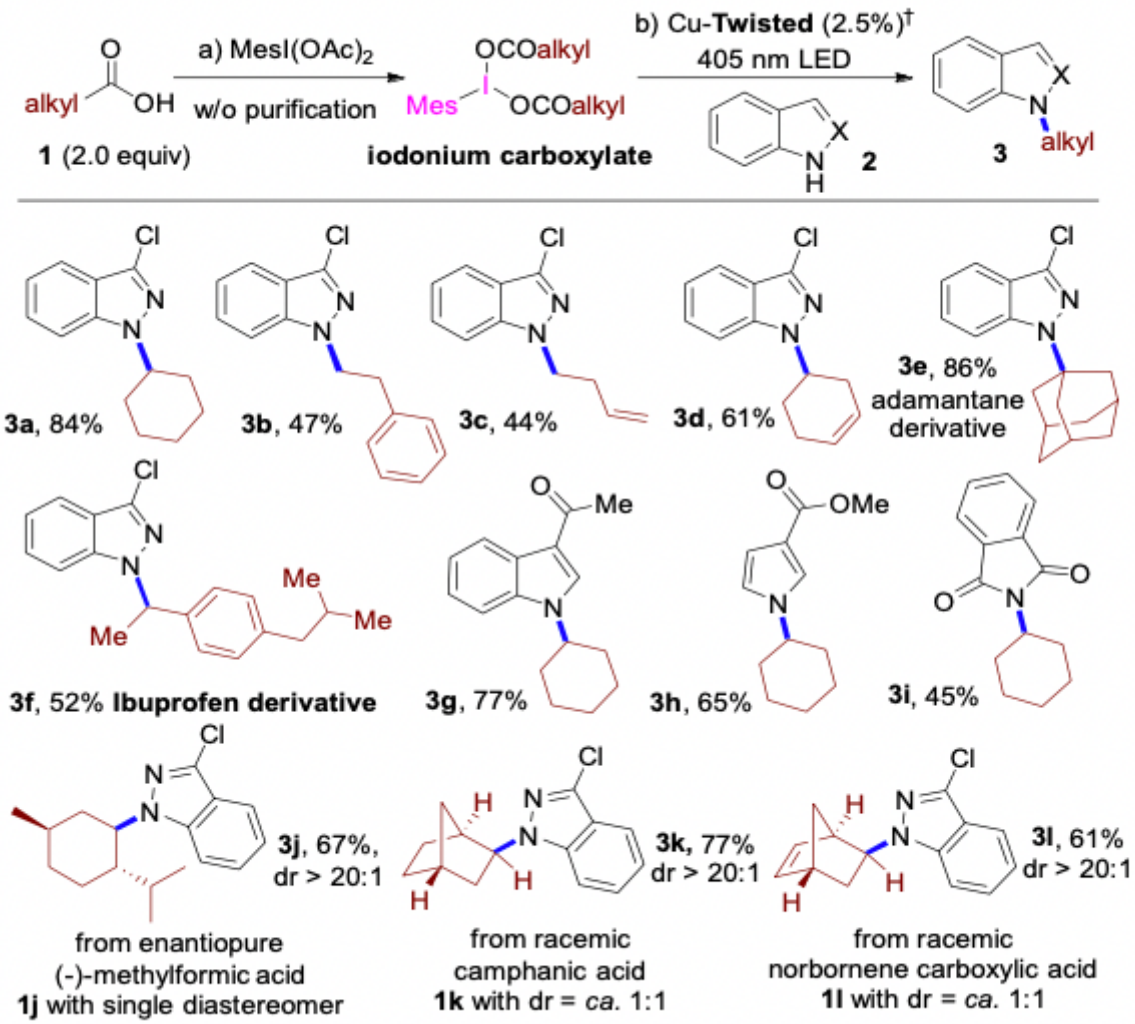

Figure 4

Heterogeneous decarboxylative C(sp3)–N coupling of iodonium carboxylates and N-nucleophiles by Cu–Twisted. †Conditions: iodonium carboxylate prepared from 1 (2.0 equiv.), N-nucleophile 2 (0.3 mmol, 1.0 equiv.), Cu–Twisted (2.5%), BTMG (2.0 equiv.), dioxane (0.05 M), 405 nm LED, N2, room temperature (r.t.), 5h. Isolated yields.

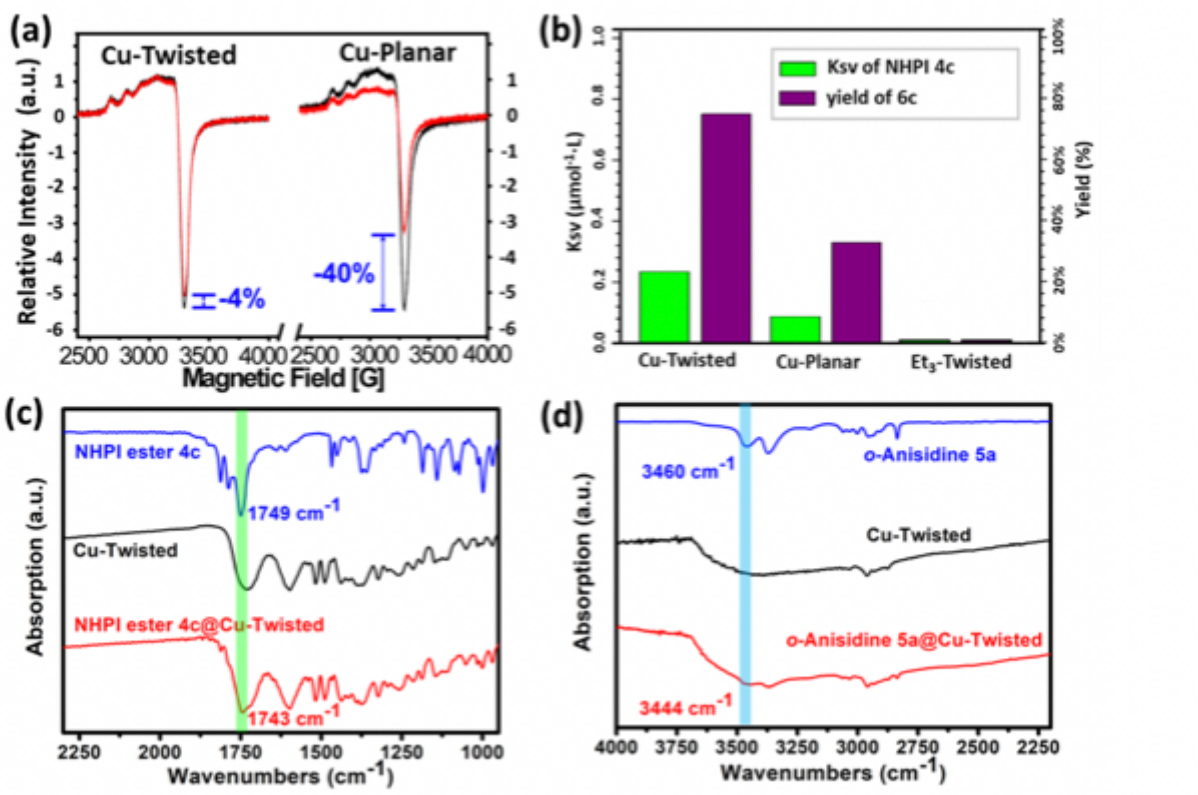

Figure 5

Cu(II) sites of Cu(II)–TPA coordination polymers retained in PET process and their coordination activations towards radical precursors and heteroatom-centred nucleophiles. a, Comparison of EPR spectra of Cu–Twisted and Cu–Planar. b, Comparison of fluorescence quenching (upon addition of NHPI ester 4c) and catalytic efficiencies of Cu–Twisted, Cu–Planar, and the ester form of free ligand, respectively. c, IR spectra of NHPI ester 4c (blue), Cu–Twisted (black), Cu–Twisted with absorbed 4c (red). The ester stretching vibrations of free and adsorbed 4c were highlighted by the inserted green band. d, IR spectra of aniline derivative 5a (blue), Cu–Twisted (black), Cu–Twisted with absorbed 5a (red). The N–H stretching vibrations of free and adsorbed 5a were highlighted by the inserted sky-blue band.

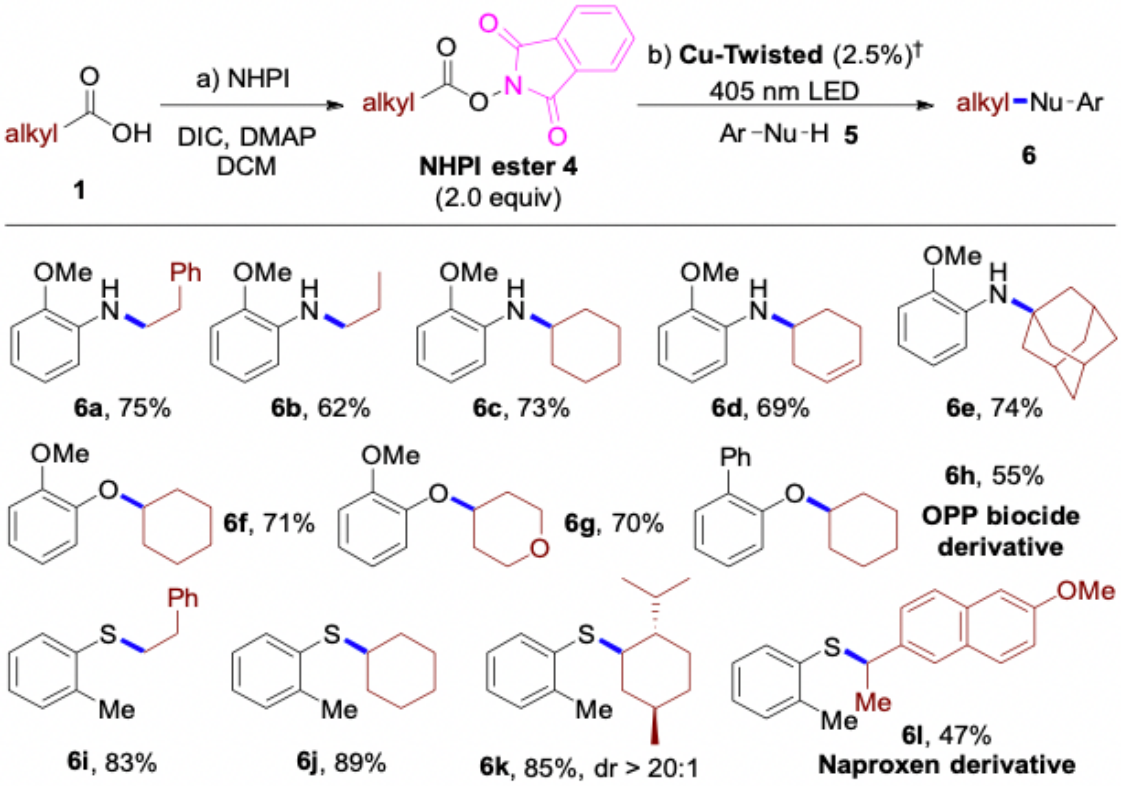

Figure 6

Heterogeneous decarboxylative C(sp3)-heteroatom coupling of NHPI esters and heteratom centred-nucleophiles by Cu–Twisted. †Conditions: Cu–Twisted (2.5%), 5 (0.3 mmol, 1.0 equiv.), 4 (2.0 equiv.), DIPEA (3.0 equiv), MeCN (0.1 M), 405 nm LED, N2, r.t., 12h. Isolated yields.

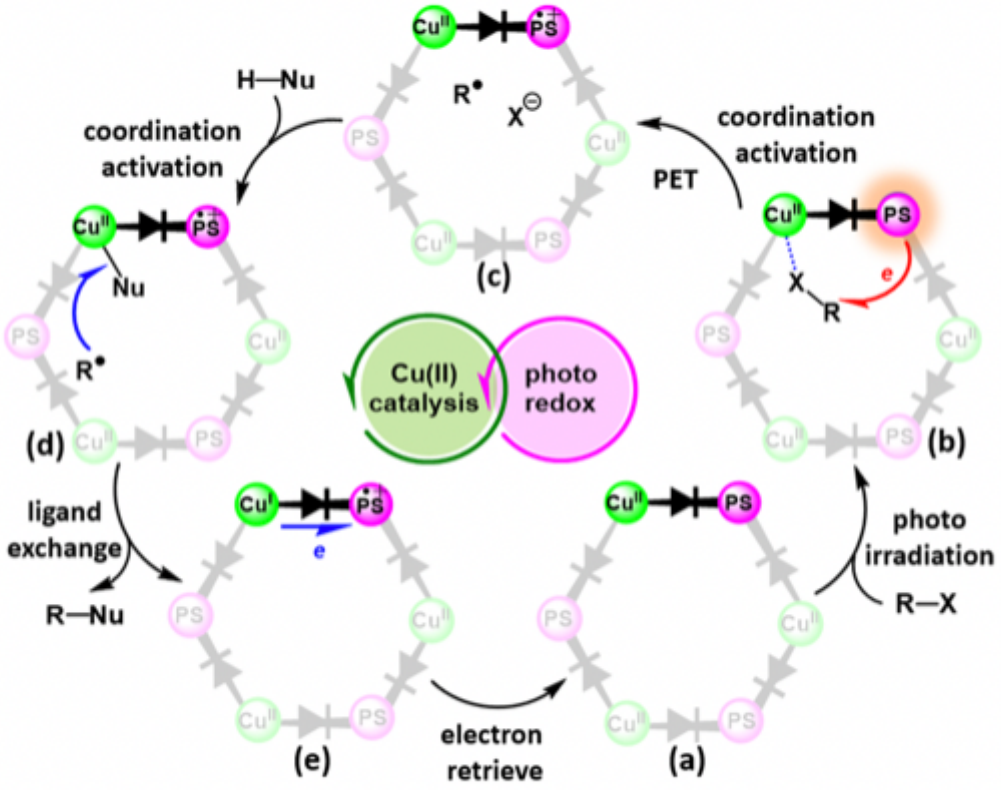

Figure 7

Proposed mechanism of synergistic photoredox and copper catalytic decarboxylative C(sp3)-heteroatom coupling by the diode-like coordination polymer Cu–Twisted.

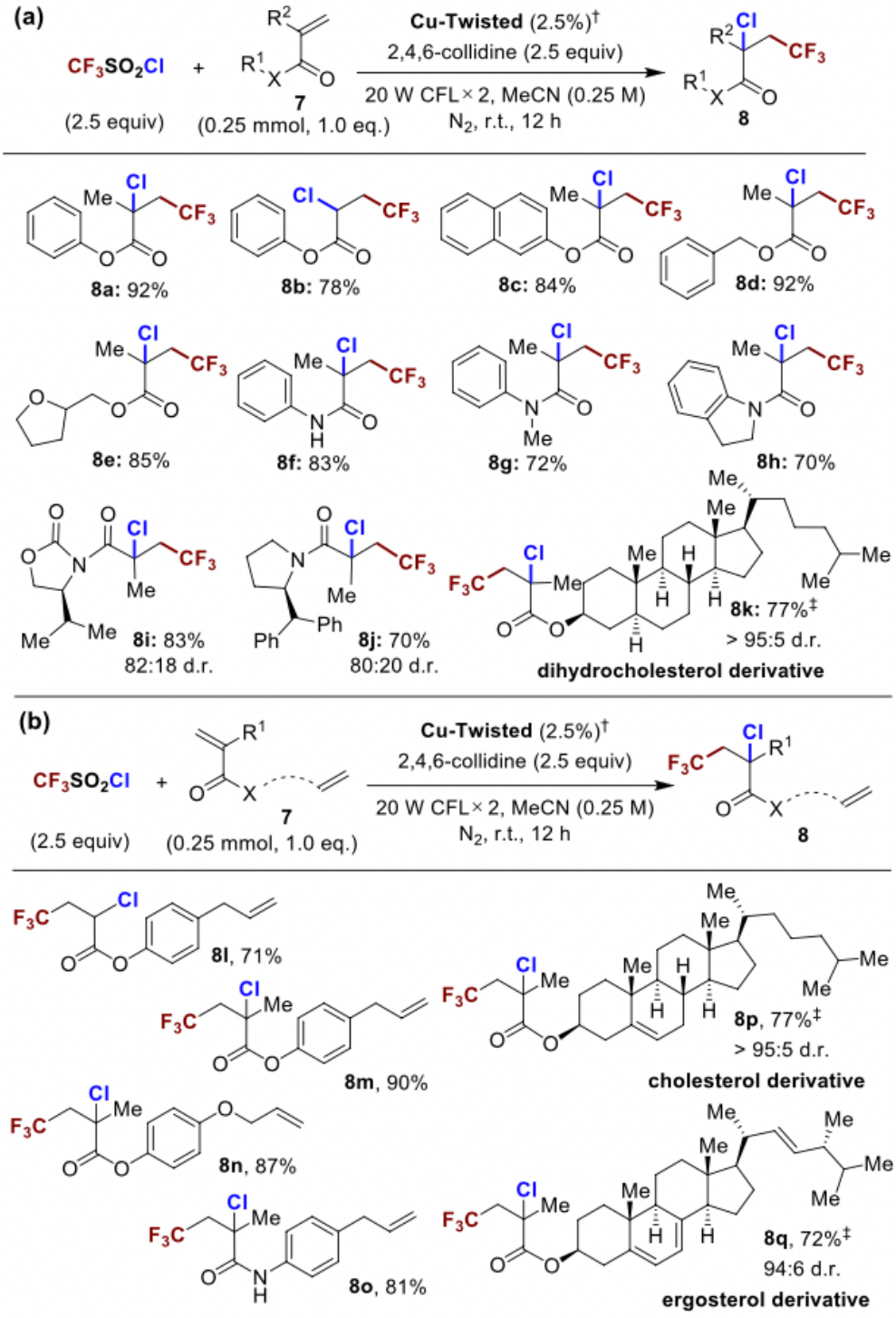

Figure 8

Heterogeneous photoredox and copper catalytic trifluoromethylation-chloration difunctionalisation by Cu–Twisted. a, Substrate scope of α,β-unsaturated esters and amides. b, Discrimination of multiple olefinic sites in difunctionalisation. †Conditions: 7 (0.25 mmol, 1.0 equiv.), TfCl and collidine (2.5 equiv.), Cu–Twisted (2.5%), MeCN (0.25 M), two 20-W CFLs, N2 atmosphere, r.t., 12 h. Isolated yields. ‡1,2-Dichloroethane as the solvent.

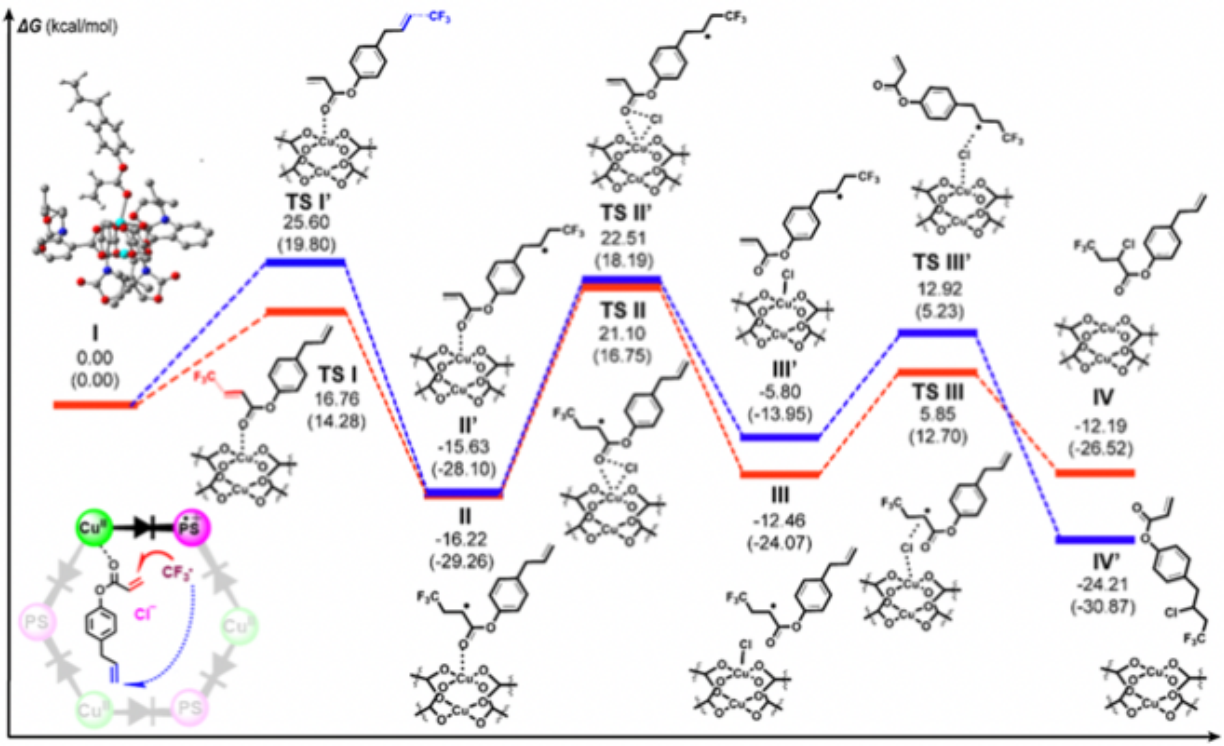

Figure 9

DFT calculated energy profiles of the reactions on the olefinic site that adjacent to carbonyl group (red) and carbonyl-free olefin terminal (blue) of 7l, which were calculated at the B3LYP/6-31G(d)-LANL2DZ level. The relative free energies and electronic energies (in parentheses) are given in kcal•mol-1. Inset, upper left (intermediate I): simplified DFT model of 7l adsorbed on the Cu(II) node. Inset, lower left: conceptual illustration of the Hammond postulate model showing the product-like late transition state in the cage. Cu, cyan; C, grey; O, red; N, blue; H atoms were omitted for clarity.

Supplementary Files

This is a list of supplementary files associated with this preprint. Click to download.

- SupplementaryInformationforNatCommun20200706.pdf
- CuTwisted.cif
- CuPlanar1870816.cif